Emergent structures in reaction-advection-diffusion systems on a sphere

Andrew L. Krause, Abigail M. Burton, Nabil T. Fadai, and Robert A. Van Gorder*
Mathematical Institute, University of Oxford, Andrew Wiles Building, Radcliffe Observatory Quarter, Woodstock Road, Oxford OX2 6GG, United Kingdom

(Received 27 September 2017; revised manuscript received 3 March 2018; published 23 April 2018)

We demonstrate unusual effects due to the addition of advection into a two-species reaction-diffusion system on the sphere. We find that advection introduces emergent behavior due to an interplay of the traditional Turing patterning mechanisms with the compact geometry of the sphere. Unidirectional advection within the Turing space of the reaction-diffusion system causes patterns to be generated at one point of the sphere, and transported to the antipodal point where they are destroyed. We illustrate these effects numerically and deduce conditions for Turing instabilities on local projections to understand the mechanisms behind these behaviors. We compare this behavior to planar advection which is shown to only transport patterns across the domain. Analogous transport results seem to hold for the sphere under azimuthal transport or away from the antipodal points in unidirectional flow regimes.

DOI: 10.1103/PhysRevE.97.042215

I. INTRODUCTION

Since Turing's original pioneering work in morphogenesis [1], there have been numerous extensions to the basic reaction-diffusion patterning mechanism, some of which are reviewed in Ref. [2]. One extension of the traditional mechanism is to consider the influence of advection on reaction-diffusion systems, whereby the interacting chemicals are transported along by some process. These reaction-advection-diffusion models have been studied from many different perspectives with a variety of forms of advection. The authors in Ref. [3] investigated reactive flows as a way of introducing inexact phase differences within Turing patterns and suggested that this is one way of encoding additional information into a biological patterning process that is more robust than traditional Turing instabilities. Similarly, Ref. [4] demonstrated Turing patterns with equal diffusion coefficients not possible in a purely reaction-diffusion system. These models are commonly used to model patterning processes when advection is present due to the physical environment, such as Ref. [5], which investigates cell aggregation due to phyllotaxis, and Refs. [6,7], where patterning of populations occurs due to directed motion (modeled as advection) and spatial heterogeneity. Novel mechanisms and patterns have also been explored experimentally [8,9] and traveling wave analyses have been carried out [10]. Finally, this class of model has also been used to explain chemical-mechanical coupling in particular organisms, such as the rhythmic contraction of the plasmodium of *Physarum polycephalum* [11]. Differential advection itself has been shown to initiate traveling-wave instabilities in models of chemical systems [12], and this has been further related to Turing-type instabilities in the case of an immobile inhibitor [13].

Another variation, first considered in Turing's original paper, is to extend the theory to curved domains, and in particular, to the sphere. This has been pursued by many authors from various directions [14]. Turing patterns have been studied on the sphere, with biological applications on embryological constraints [15] and the growth of solid tumours [16] considered. Several authors have considered the effect that spherical geometry has had on the existence and stability of particular solutions, such as localized spot patterns and their transient formation [17–19]. Many of these models are motivated by specific biological applications, such as membrane-protein interactions [20] and in both developing embryos and the mitosis of a single cell [21]. Extensions to more general manifolds have been considered from both theoretical [22–24] and experimental [25] perspectives.

We are chiefly motivated by novel features present in a reaction-diffusion system on a compact surface introduced via advection of the constituents across the surface. This framework captures many existing models and extends others in a natural way. There are many physical and biological phenomena that can be modelled by reaction-advection-diffusion systems on a sphere, or more generally on the surface of curved manifolds. In atmospheric physics, reaction-advection-diffusion systems with spherical geometries have been used to model the transport of water across the surface of the earth [26,27], as well as to model chemical transport due to atmospheric convection [28,29]. Similar atmospheric models have also been used to model the transport of microorganisms (e.g., bacteria, [30,31]), as well as dust in arid environments [32].

While we are not aware of reaction-advection-diffusion models in physiology or developmental biology, we believe that this more general setting would be a useful framework within which to extend questions about protein binding on cell surfaces [20], or to investigate the effect of flow through or past a solid tumor [16]. Growing geometries have been shown to give rise to advection-like terms [23,33,34], and analysis of our generic system will lend insight into the behavior of these kinds of models in general.

*robert.vangorder@maths.ox.ac.uk

Lastly, we mention that many kinds of active transport of, e.g. cells, are possible that give rise to advection terms in the governing equations for a population. For example, if the advection is due to the gradients of a function of some given chemical field, then this can model chemotaxis [35,36]. Similar remarks can be made about many other forms of cell movement, such as rheotaxis in the presence of flow [37], phyllotaxis in the presence of light [38,39], or even magnetotaxis in the presence of an external electromagnetic field [40]. Nonlinear advection has been shown to introduce oscillatory instabilities in reaction-convection-diffusion systems as well [41]. While these various forms of cell taxes and other nonlinear forms of advection have been studied on planar two-dimensional domains, we show in this paper that considering them on the surface of a sphere leads to new kinds of population-level behavior, even under the simplification of simple linear advection. We note that linearity here is with respect to the unknown chemical species, and that we will consider both homogeneous and inhomogeneous forms of advection.

Consider the nondimensional two-species reaction-advection-diffusion system on the surface of a sphere of radius R (so that $\mathbf{x} \in \mathcal{S}^2 \subset \mathbb{R}^3$) given by

$$\frac{\partial u}{\partial t} = \frac{\delta_1}{R^2}\triangle u - \frac{1}{R}\nabla \cdot [\mathbf{A}(\mathbf{x})u] + f(u,v), \tag{1}$$

$$\frac{\partial v}{\partial t} = \frac{\delta_2}{R^2}\triangle v - \frac{1}{R}\nabla \cdot [\mathbf{B}(\mathbf{x})v] + g(u,v), \tag{2}$$

where u, v are the interacting species, f, g are nonlinear kinetic functions, $\mathbf{A}$, $\mathbf{B}$ determine the advective component of transport, and δ_1, δ_2 are diffusion coefficients. In spherical coordinates, $\mathbf{x} = (\theta,\phi)$, and the Laplace-Beltrami and tangential divergence operators are defined as

$$\triangle u = \frac{1}{\sin(\theta)}\left\{\frac{\partial}{\partial\theta}\left[\sin(\theta)\frac{\partial u}{\partial\theta}\right] + \frac{1}{\sin(\theta)}\frac{\partial^2 u}{\partial\phi^2}\right\}, \tag{3}$$

$$\nabla \cdot \mathbf{A} = \frac{1}{\sin(\theta)}\left\{\frac{\partial}{\partial\theta}[\sin(\theta)A_\theta] + \frac{\partial A_\phi}{\partial\phi}\right\}, \tag{4}$$

where $\mathbf{A} = (A_\theta, A_\phi)$ [16,42].

Equations (1)–(2) represent a general reaction-advection-diffusion system that contains many specific submodels. Nonlinear generalizations of this advection term also give rise to interesting behavior, but for the remainder of this paper, we will concentrate on linear (possibly inhomogeneous) advection to demonstrate the interplay this transport mechanism has with the spherical geometry. We shall consider reaction-advection-diffusion systems on the sphere to understand how these variations on the classical Turing pattern-formation mechanism interact with one another. In Sec. II we give generic instability results for spatially uniform equilibria with strong assumptions on the advection. Due to difficulties raised in this general analysis, we proceed to consider a caricature of the regions present in a unidirectional flow regime in Sec. III in order to make analytical progress. We then systematically investigate model behaviors in Sec. IV. We demonstrate novel behaviors of advection on a sphere (which is an example of a compact manifold without boundary) and discuss these behaviors in terms of spectral theory and small-diffusion asymptotics. We consider Schnakenberg [43], Geirer-Meinhardt [44], and FitzHugh-Nagumo [45] kinetics to show that these behaviors are generic within some regions of the Turing space, depending on the magnitude and form of the advection. Finally, we discuss mathematical and biological implications of our work in Sec. V.

II. STABILITY PROBLEM FOR SPATIALLY UNIFORM STEADY STATES ON THE SPHERE

Let $(u^*,v^*) \in \mathbb{R}^2$ be a spatially uniform steady state such that $f(u^*,v^*) = 0$ and $g(u^*,v^*) = 0$. Consider a small perturbation of these steady states, $u = u^* + \epsilon\bar{u}$, $v = v^* + \epsilon\bar{v}$, for $0 < \epsilon \ll 1$. In order for (1)–(2) to admit spatially uniform steady states corresponding to the steady states of the reaction kinetics, we must have divergence-free advection vectors, i.e., $\nabla \cdot \mathbf{A} = 0$ and $\nabla \cdot \mathbf{B} = 0$. In this case, the advection term only involves gradients of u or v which vanish on a spatially uniform state.

We first focus on the case where $\delta_1 = \delta_2 = 0$, $\mathbf{A} = \mathbf{B} = \mathbf{0}$, i.e., the case of reaction kinetics only. Then setting $f_u = \frac{\partial f}{\partial u}(u^*,v^*)$, $f_v = \frac{\partial f}{\partial v}(u^*,v^*)$, $g_u = \frac{\partial g}{\partial u}(u^*,v^*)$, $g_v = \frac{\partial g}{\partial v}(u^*,v^*)$ we get

$$\frac{d}{dt}\begin{pmatrix}\bar{u}\\ \bar{v}\end{pmatrix} = \tilde{J}\begin{pmatrix}\bar{u}\\ \bar{v}\end{pmatrix}, \tag{5}$$

where

$$\tilde{J} = \begin{pmatrix} f_u & f_v \\ g_u & g_v \end{pmatrix}. \tag{6}$$

This linear system is stable provided $\mathrm{tr}(\tilde{J}) = f_u + g_v < 0$ and $\det(\tilde{J}) = f_u g_v - f_v g_u > 0$ [2]. We shall always assume these criteria on the reaction kinetics are satisfied.

To address the influence of spatial perturbations, consider now $\delta_1,\delta_2 > 0$, $\mathbf{A},\mathbf{B} \neq \mathbf{0}$. Spatio-temporal perturbations of the spatially uniform steady states may then be written in the form

$$u(\mathbf{x},t) = u^* + \epsilon\sum_\ell \sigma_{u,\ell} e^{\lambda_\ell t} Y_\ell(\mathbf{x}) \exp[\mathcal{A}(\mathbf{x})], \tag{7}$$

$$v(\mathbf{x},t) = v^* + \epsilon\sum_\ell \sigma_{v,\ell} e^{\lambda_\ell t} Y_\ell(\mathbf{x}) \exp[\mathcal{A}(\mathbf{x})], \tag{8}$$

where $Y_\ell(\mathbf{x})$ is a spherical harmonic for $\mathcal{S}^2 \subset \mathbb{R}^3$, with eigenvalue $\lambda_\ell = -\frac{\ell(\ell+1)}{R^2}$ (which may appear with multiplicity greater than one), $\sigma_{u,\ell}$ and $\sigma_{v,\ell}$ are arbitrary constants corresponding to an eigenfunction expansion of the perturbation, $\mathbf{x} \in \mathcal{S}^2$, and $\mathcal{A}(\mathbf{x})$ is a function which satisfies

$$\nabla\mathcal{A} = \frac{R}{2\delta_1}\mathbf{A}. \tag{9}$$

The function $\mathcal{A}$ can be interpreted as the scalar potential for $\mathbf{A}$, the existence of which is guaranteed as $\mathbf{A}$ is assumed divergence-free. The factor of $\exp[\mathcal{A}(\mathbf{x})]$ is therefore motivated by integrating factors for ordinary differential equations. For consistency of our equations, we assume $\mathbf{B}(\mathbf{x}) = \frac{\delta_2}{\delta_1}\mathbf{A}(\mathbf{x})$. We shall also assume $|\mathbf{A}|$ is constant on the sphere, corresponding to a constant magnitude advection over the surface of the sphere.

Placing (7)–(8) into the linearized problem for (1)–(2), we obtain

$$\lambda_\ell\begin{pmatrix}\sigma_{u,\ell}\\ \sigma_{v,\ell}\end{pmatrix} = J_\ell\begin{pmatrix}\sigma_{u,\ell}\\ \sigma_{v,\ell}\end{pmatrix}, \tag{10}$$

where

$$J_\ell = \begin{pmatrix} -\frac{\delta_1}{R^2}\ell(\ell+1) - \frac{|\mathbf{A}|^2}{2\delta_1} + f_u & f_v \\ g_u & -\frac{\delta_2}{R^2}\ell(\ell+1) - \frac{\delta_2}{\delta_1}\frac{|\mathbf{A}|^2}{2\delta_1} + g_v \end{pmatrix}. \tag{11}$$

As $\mathrm{tr}(J_\ell) \leqslant \mathrm{tr}(\tilde{J}) < 0$, and $\det(\tilde{J}) > 0$ by assumption, a necessary condition for the Turing instability is that $\det(J_\ell) < 0$ for some integer $\ell > 0$. We note that this condition is a simple modification of the classical necessary conditions for diffusion-driven instability in reaction-diffusion systems; see Ref. [2] for a general treatment of conditions for diffusion-driven instability, and Refs. [46–48] for contemporary examples of Turing instability conditions comparable to our analysis above.

Note that we have relied on the assumption that $|\mathbf{A}|$ is constant. Attempting to relax this restriction, we find that we obtain a spatially heterogeneous linear eigenvalue problem, for which determining the spectrum is not tractable in general. This therefore leads us to consider a simplification in the geometry of the problem. This shall allow us to study advective sources or sinks, for which $|\mathbf{A}|$ is not constant. We note that the analysis in the following section will not rigorously correspond to a stability analysis of the full problem, but is instead a caricature which is meant to give some insight into the behavior of the reaction-advection-diffusion system.

III. CURVATURE-FREE LOCAL APPROXIMATIONS OF TURING INSTABILITY CRITERIA IN THREE REGIONS OF IMPORTANCE

In order to analytically approximate the mechanism for Turing instability on the sphere due to advection in a more general setting where $|\mathbf{A}|$ and $|\mathbf{B}|$ are not necessarily constant, we shall approximate the salient dynamics on the sphere $\mathcal{S}^2$ by considering three regions. In this analysis, the advection shall originate at a point P_1 on the sphere, with the advective flow then tending to the antipodal point P_2. Under the divergence-free assumption on the vector fields $\mathbf{A}$ and $\mathbf{B}$, this results in an advection diverging from P_1 and converging to P_2. We shall take Region I to be a circular cap of radius $0 < \rho \ll R$ centered about P_1; as $\rho \ll R$ we shall assume curvature effects are negligible and consider the geometry to be that of a disk on the plane $\mathbb{R}^2$. We then consider an intermediate cylindrical Region II, in which the two species are advected along the sphere along fixed streamlines after they leave Region I. There is a corresponding Region III centered about P_2 with radius $0 < \rho \ll R$, and the species are advected into this region after they pass through Region II. As with Region I, we shall assume Region III is a disk in the plane, neglecting any curvature effects. In this way, Regions I and III are really disks lying in the tangent plane to the sphere at points P_1 and P_2, respectively. See Fig. 1 for an illustration of these regions and their corresponding idealizations. While this decomposition is a crude approximation of the sphere, we show later that the analytical results derived from these approximations do indeed show agreement with numerical simulations for the full problem on the true curved spherical geometry.

A. Dynamics on Regions I and III

We start with Regions I and III, modeling each as a disk with radius $0 < \rho \ll R$. Note that Region I will act as a source, and Region III as a sink. Hence, it is sensible to assume purely radial spatial coordinates for both the advection and solution functions. Taking $u = u(r,t)$ and $v = v(r,t)$, (1)–(2) give

$$\frac{\partial u}{\partial t} = \delta_1 \frac{1}{r}\frac{\partial}{\partial r}\left(r\frac{\partial u}{\partial r}\right) - \frac{1}{r}\frac{\partial}{\partial r}(rA(r)u) + f(u,v), \tag{12}$$

$$\frac{\partial v}{\partial t} = \delta_2 \frac{1}{r}\frac{\partial}{\partial r}\left(r\frac{\partial v}{\partial r}\right) - \frac{1}{r}\frac{\partial}{\partial r}(rB(r)v) + g(u,v). \tag{13}$$

We are interested in showing that these regions give rise to local instability from uniform steady state solutions, and so relevant boundary conditions for Regions I and III are

$$u = u^*, \quad v = v^* \quad \text{at} \quad r = \rho\,, \tag{14}$$

$$\frac{\partial u}{\partial r} = 0\,, \quad \frac{\partial v}{\partial r} = 0 \quad \text{at} \quad r = 0\,. \tag{15}$$

Assume that there exists a spatially uniform steady state (u^*,v^*) satisfying $f(u^*,v^*) = g(u^*,v^*) = 0$. For this, we require that $\nabla \cdot \mathbf{A} = 0, \nabla \cdot \mathbf{B} = 0$. However, this is equivalent to $\frac{1}{r}\frac{\partial}{\partial r}(rA(r)) = 0$, so that $A(r) = \frac{A_0}{r}$ and, similarly, $B(r) = \frac{B_0}{r}$. We choose the constants A_0 and B_0 to be positive in Region I and negative in Region III to correspond to source and sink dynamics respectively. We perturb the spatially uniform steady states as

$$u = u^* + \epsilon\sigma_u e^{\lambda t} W(r) + O(\epsilon^2), \tag{16}$$

$$v = v^* + \epsilon\sigma_v e^{\lambda t} W(r) + O(\epsilon^2), \tag{17}$$

where σ_u and σ_v are arbitrary nonzero constants [which are $O(1)$ in ϵ], $W(r)$ is an eigenfunction, and λ is the temporal

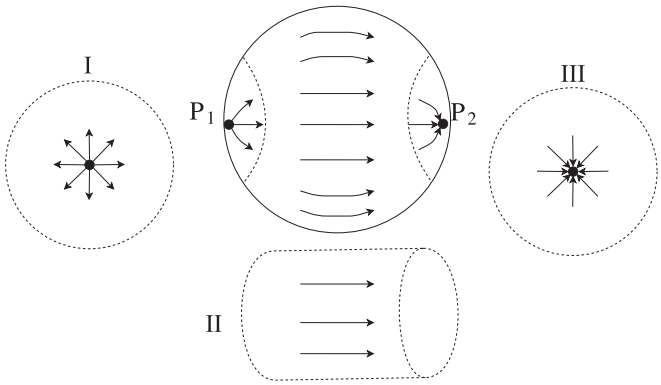

FIG. 1. A diagram of the three regions analyzed in Sec. III, showing how they relate to unidirectional flow on the sphere. We consider a local disk tangent to the sphere at each antipode, and then a cylindrical region along the center of the sphere.

eigenvalue. Placing these into (12)–(13), we obtain the eigenvalue problem for the perturbations, which takes the form

$$\delta_1 \frac{1}{r}\frac{d}{dr}\left(r\frac{dW}{dr}\right) - \frac{A_0}{r}\frac{dW}{dr} = \mu W\,, \tag{18}$$

subject to the solvability condition $B_0 = \frac{\delta_2}{\delta_1}A_0$. For the perturbed problem, the boundary conditions become

$$W = 0 \quad \text{at } r = \rho, \tag{19}$$

$$\frac{dW}{dr} = 0 \quad \text{at } r = 0. \tag{20}$$

Assuming such a solution $W(r)$ to our boundary value problem exists and has eigenvalues μ, we obtain the linear system

$$\lambda\begin{pmatrix}\sigma_u\\ \sigma_v\end{pmatrix} = \begin{pmatrix}\mu + f_u & f_v\\ g_u & \frac{\delta_2}{\delta_1}\mu + g_v\end{pmatrix}\begin{pmatrix}\sigma_u\\ \sigma_v\end{pmatrix}. \tag{21}$$

Let $\mu = -k^2$ and set $\alpha = \frac{1}{2}\frac{A_0}{\delta_1}$, $\beta = \frac{k}{\sqrt{\delta_1}}$. Solving Eq, (18), we get

$$R(r) = \{C_1 J_{-\alpha}(\beta r) + C_2 Y_{-\alpha}(\beta r)\}r^{\alpha}\,, \tag{22}$$

where J and Y denote Bessel functions of first and second kind, respectively [49]. Implementation of the boundary condition at $r = 0$ will depend on the value of α, as

$$\frac{dR}{dr} = -\beta\{C_1 J(1-\alpha,\beta r) + C_2 Y(1-\alpha,\beta r)\}r^{\alpha} \tag{23}$$

and $\lim_{r\to 0} r^{\alpha}J(1-\alpha,\beta r) = 0$ for all $\alpha \in \mathbb{R}$, while $\lim_{r\to 0} r^{\alpha}Y(1-\alpha,\beta r) = 0$ only if $\alpha > \frac{1}{2}$, with the limit nonzero (and, in some cases, singular) otherwise.

First, we consider the case $\alpha \leqslant \frac{1}{2}$, which then gives $C_2 = 0$. Using the remaining boundary condition, we have $J_{-\alpha}(\beta\rho) = 0$. Let $j_{-\alpha,n}$ be the nth root of the Bessel function J_{α} for $n = 1,2,\ldots$. We then obtain $\mu_n = -k_n^2$, where $k_n = \frac{\sqrt{\delta_1}}{\rho}j_{-\frac{1}{2}\frac{A_0}{\delta_1},n}$. This puts the spectral problem into the form

$$\lambda_n\begin{pmatrix}\sigma_u\\ \sigma_v\end{pmatrix} = J_n\begin{pmatrix}\sigma_u\\ \sigma_v\end{pmatrix}, \tag{24}$$

where

$$J_n = \begin{pmatrix}-\frac{\delta_1}{\rho^2}(j_{-\frac{1}{2}\frac{A_0}{\delta_1},n})^2 + f_u & f_v\\ g_u & -\frac{\delta_2}{\rho^2}(j_{-\frac{1}{2}\frac{A_0}{\delta_1},n})^2 + g_v\end{pmatrix}. \tag{25}$$

Recall $\tilde{J}$ as defined in (6) with $\mathrm{tr}(\tilde{J}) < 0$ and $\det(\tilde{J}) > 0$ for stability. Then this implies that $\mathrm{tr}(J_n) < 0$ for any n, so we require that $\det(J_n) < 0$ for some n in order for there to be a Turing instability.

Next, we consider the case $\alpha > \frac{1}{2}$. Note that $\frac{dW}{dr}|_{r=0} = 0$ for $\alpha > \frac{1}{2}$ without the need to set either C_1 or C_2 to zero, so the remaining boundary condition $W(\rho) = 0$ yields

$$C_2 = -C_1\frac{J(-\alpha,\beta\rho)}{Y(-\alpha,\beta\rho)}. \tag{26}$$

We have not fixed a discrete spectrum, meaning that any $k \in \mathbb{R}$ serves as an eigenvalue, i.e., that the spectrum is continuous with $\mu = -k^2$ for $k \in \mathbb{R}$. The spectral problem is then

$$\lambda\begin{pmatrix}\sigma_u\\ \sigma_v\end{pmatrix} = J(k)\begin{pmatrix}\sigma_u\\ \sigma_v\end{pmatrix}, \tag{27}$$

where

$$J(k) = \begin{pmatrix}-k^2 + f_u & f_v\\ g_u & -k^2 + g_v\end{pmatrix}. \tag{28}$$

Observe that $J(0) = \tilde{J}$, $\mathrm{tr}(\tilde{J}) < 0$, and $\det(\tilde{J}) > 0$, hence $\mathrm{tr}(J(k)) \leqslant \mathrm{tr}(\tilde{J}) < 0$ for all $k \in \mathbb{R}$. The condition for the Turing instability is then the existence of an interval (k_1,k_2), with $0 < k_1 < k_2 < \infty$, for which $\det[J(k)] < 0$ for all $k \in (k_1,k_2)$.

In summary, when $A_0 \leqslant \delta_1$, the condition for the Turing instability in Region I or III is

$$\det(J_n) = \frac{\delta_1\delta_2}{\rho^4}(j_{-\frac{1}{2}\frac{A_0}{\delta_1},n})^4 - \frac{\delta_1 g_v + \delta_2 f_u}{\rho_2}(j_{-\frac{1}{2}\frac{A_0}{\delta_1},n})^2 + \det(\tilde{J}) < 0, \tag{29}$$

for some $n = 1,2,\ldots$, while when $A_0 > \delta_1$ the condition for the Turing instability is

$$\det[J(k)] = k^4 - \mathrm{tr}(\tilde{J})k^2 + \det(\tilde{J}) < 0 \tag{30}$$

for all $k \in (k_1,k_2)$, provided there exist k_1 and k_2 satisfying $0 < k_1 < k_2 < \infty$.

To place these results into context, for $A_0 \leqslant \delta_1$ (the diffusion-dominated limit), we obtain a discrete spectrum, while for $A_0 > \delta_1$ (the advection-dominated limit), we obtain a continuous spectrum. If such k_1 and k_2 exist, then the continuous spectrum problem will always have excited modes, while a corresponding discrete spectrum may not, depending on if one of the discrete eigenvalues satisfies the condition given above. For instance, it can be shown that

$$j_{-\alpha,n} \xrightarrow[n\to\infty]{} \pi\left(n + \frac{3}{4} - \frac{\alpha}{2}\right) \quad \text{for } \alpha \leqslant 0, \tag{31}$$

$$j_{-\alpha,n} \xrightarrow[n\to\infty]{} \pi\left(n + \frac{3}{4} + \frac{\alpha}{2}\right) \quad \text{for } \alpha \in \mathbb{Z}_{\geqslant 0}, \tag{32}$$

$$j_{-\alpha,n} \xrightarrow[n\to\infty]{} \pi\left(n + \frac{1}{4} + \frac{\alpha}{2}\right) \quad \text{for } \alpha \in \mathbb{Z}_{\geqslant 0} + \frac{1}{2}, \tag{33}$$

$$j_{-\alpha,n} \xrightarrow[n\to\infty]{} \pi\left(n + \frac{3}{4} - \frac{\alpha}{2}\right) \quad \text{otherwise}, \tag{34}$$

where the order of convergence is $O(\frac{1}{n})$. Therefore, it may be the case that the discrete spectrum always results in a positive determinant, while a corresponding continuous spectrum gives some interval on which the determinant is negative if that interval falls within a gap in the discrete spectrum.

B. Dynamics on Region II

We now turn our attention to Region II, which we model as a cylinder of length L and radius ρ. Unlike in Regions I and III, where we assumed $0 < \rho \ll R$, for Region II, we assume $\rho = O(R)$. This geometry is a model of the central band along the sphere between the two antipodes, P_1 and P_2, and we shall assume curvature has a negligible influence on the dynamics

in this region. Mathematically, this geometry corresponds to a rectangle $(x,y) \in [0,L] \times [0,2\pi\rho]$ in the plane. We impose periodic boundary conditions

$$u(x,0,t) = u(x,2\pi\rho,t), \tag{35}$$

$$\frac{\partial u}{\partial y}(x,0,t) = \frac{\partial u}{\partial y}(x,2\pi\rho,t), \tag{36}$$

$$v(x,0,t) = v(x,2\pi\rho,t), \tag{37}$$

$$\frac{\partial v}{\partial y}(x,0,t) = \frac{\partial v}{\partial y}(x,2\pi\rho,t), \tag{38}$$

and Dirichlet boundary conditions

$$u(0,y,t) = u^* = u(L,y,t), \tag{39}$$

$$v(0,y,t) = v^* = v(L,y,t). \tag{40}$$

Consider $\mathbf{A} = A_1\hat{\mathbf{x}}$ and $\mathbf{B} = B_1\hat{\mathbf{x}}$, so that advection is in the positive x direction along the sides of the cylinder. Then (1)–(2) take the form

$$\frac{\partial u}{\partial t} = \delta_1 \Delta u - A_1 \frac{\partial u}{\partial x} + f(u,v), \tag{41}$$

$$\frac{\partial v}{\partial t} = \delta_2 \Delta v - B_1 \frac{\partial v}{\partial x} + g(u,v). \tag{42}$$

We consider a perturbation about the spatially uniform steady state of the form

$$u = u^* + \epsilon\bar{u}, \tag{43}$$

$$v = v^* + \epsilon\bar{v}, \tag{44}$$

where $|\epsilon| \ll 1$, and the eigenfunction expansions are of the form

$$\bar{u} = \sum_{m,n} \sigma_{u,m,n} e^{\lambda_{m,n}t} \sin\left(\frac{m\pi x}{L}\right) \exp\left(\frac{A_1}{2\delta_1}\right) \times \left\{ p_n \sin\left(\frac{ny}{\rho}\right) + q_m \cos\left(\frac{ny}{\rho}\right) \right\}, \tag{45}$$

$$\bar{v} = \sum_{m,n} \sigma_{v,m,n} e^{\lambda_{m,n}t} \sin\left(\frac{m\pi x}{L}\right) \exp\left(\frac{A_1}{2\delta_1}\right) \times \left\{ p_n \sin\left(\frac{ny}{\rho}\right) + q_m \cos\left(\frac{ny}{\rho}\right) \right\}. \tag{46}$$

The consistency condition is found to be $B_1 = \frac{\delta_2}{\delta_1} A_1$. Using (45)–(46) to linearize (41)–(42), we obtain for each m,n pair the system

$$\lambda_{m,n} \begin{pmatrix} \sigma_{u,m,n} \\ \sigma_{v,m,n} \end{pmatrix} = J_{m,n} \begin{pmatrix} \sigma_{u,m,n} \\ \sigma_{v,m,n} \end{pmatrix}, \tag{47}$$

where

$$J_{m,n} = \begin{pmatrix} -\delta_1\left[\left(\frac{m\pi}{L}\right)^2 + \left(\frac{n}{\rho}\right)^2\right] - \frac{A_1^2}{2\delta_1} + f_u & f_v \\ g_u & -\delta_2\left[\left(\frac{m\pi}{L}\right)^2 + \left(\frac{n}{\rho}\right)^2\right] - \frac{\delta_2}{\delta_1}\frac{A_1^2}{2\delta_1} + g_v \end{pmatrix}. \tag{48}$$

With $\tilde{J}$ as before, we once again set $\mathrm{tr}(\tilde{J}) < 0$ and $\det(\tilde{J}) > 0$, noting that $\mathrm{tr}(J_{m,n}) \leqslant \mathrm{tr}(J_{0,0}) \leqslant \mathrm{tr}(\tilde{J}) < 0$ for all m,n. For the Turing instability, we therefore must have that $\det(J_{m,n}) < 0$ for some $m,n \in \mathbb{N}$.

C. Summary

The intuition here is that the $A_0 > \delta_1$ case can be less stable, resulting in the Turing instability even if a corresponding condition for $A_0 < \delta_1$ is not satisfied. We shall see later that $A_0 > \delta_1$ can result in generation of patterns as the two species are advected away from P_1 in Region I, while there is a collapse of patterns to a uniform state at P_2 for $A_0 < 0$ (and hence $A_0 < \delta_1$) in Region III. Region II may or may not have the Turing instability, depending on the discrete spectrum associated to $J_{m,n}$ satisfying $\det(J_{m,n}) < 0$ for some $m,n \in \mathbb{N}$. If the dynamics in Region II remain stable against perturbations, patterns created in Region I will be transported through Region II before being destroyed in Region III. On the other hand, if Region II exhibits the Turing instability, then patterns generated in Region I can evolve into new patterns while they are transported across the sphere, before entering Region III.

Note that the form of $J_{m,n}$ from (48) is similar to the Jacobian J_ℓ given on the sphere in (11). This makes sense, as we assume that the advection vectors have constant magnitude over Region II, which was a necessary condition for the result on the sphere. This suggests that the dynamics in Region II should be similar to those observed on a sphere when the advection is not strongly dependent on the spatial position. In contrast, the results for Regions I and III differ from the results for Region II and the sphere, owing to the fact that advection in those regions depends strongly on the spatial coordinates.

Doing similar analysis on a planar region with constant $\mathbf{A} = (A_x, A_y)$ and $\mathbf{B} = (B_x, B_y)$, we can conclude that a uniform steady state is stable if

$$-(\delta_1+\delta_2)|\mathbf{k}|^2 + f_u + g_v + \frac{1}{\sqrt{2}}\sqrt{\sqrt{p^2+q^2}+p} < 0\,, \tag{49}$$

where

$$p = (|\mathbf{k}|^2(\delta_1+\delta_2) - f_u - g_v)^2 - (\mathbf{k}\cdot(\mathbf{A}+\mathbf{B}))^2 - 4(\delta_1|\mathbf{k}|^2 - f_u)(\delta_2|\mathbf{k}|^2 - g_u) + 4(\mathbf{k}\cdot\mathbf{A})(\mathbf{k}\cdot\mathbf{B}) + 4f_v g_u, \tag{50}$$

$$q = -2[|\mathbf{k}|^2(\delta_1+\delta_2) - f_u - g_v][\mathbf{k}\cdot(\mathbf{A}+\mathbf{B})] - 4(\mathbf{k}\cdot\mathbf{B}) \times (\delta_1|\mathbf{k}|^2 - f_u) - 4(\mathbf{k}\cdot\mathbf{A})(\delta_2|\mathbf{k}|^2 - g_v). \tag{51}$$

This stability criterion, and the discrete nature of the spectrum for planar regions, are similar to the Region II analysis

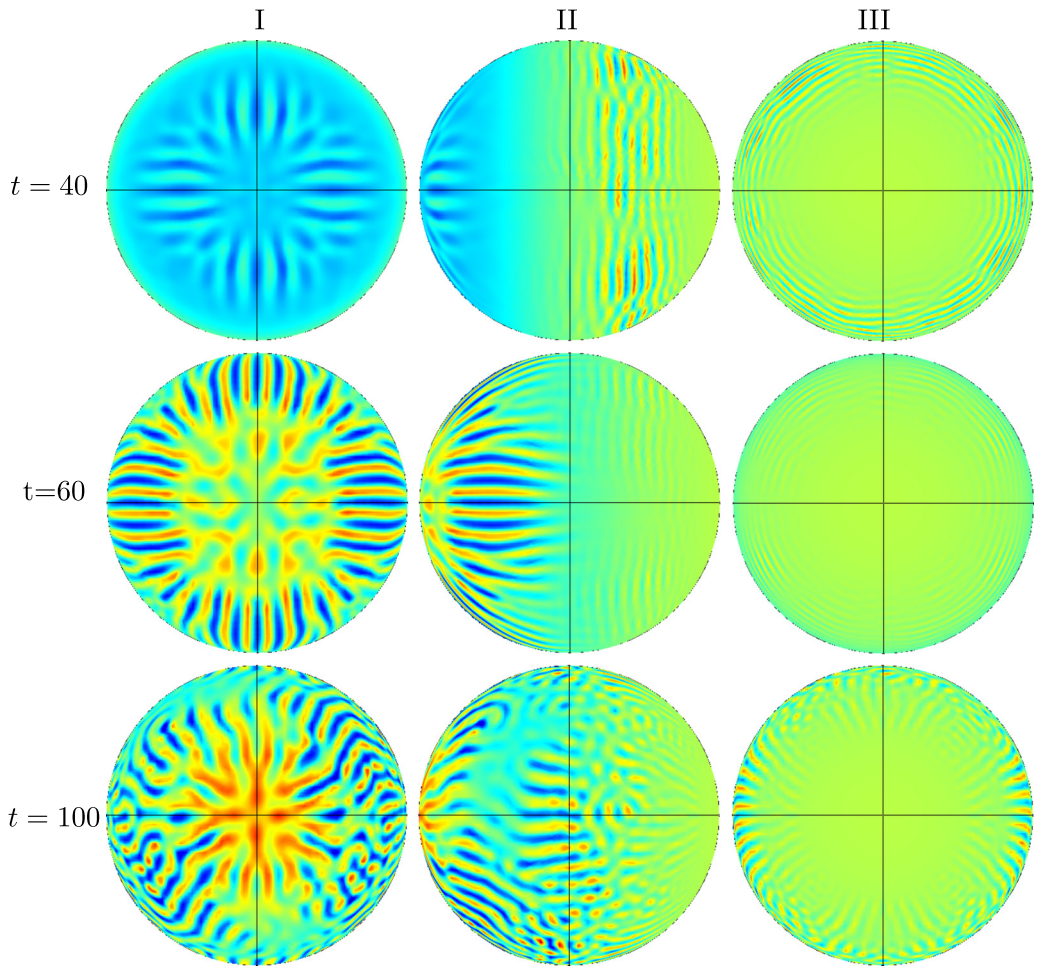

FIG. 2. Transient formation of labyrinthine patterns in the Schnakenberg model (52) with $R = 100$, $a = 0.1$, $b = 0.9$, $\delta_1 = 1$, $\delta_2 = 10$, and $A_x = 4$ for $\mathbf{A} = \mathbf{B} = A_x[-\sin(\theta)\sin(\phi), \cos(\theta)\cos(\phi)]$. The three columns are different views of source-side sink, and each row corresponds to $t = 40,60,100$.

done above. Hence, we anticipate that solution behavior in this region of the sphere is comparable to the planar setting. In particular, with the introduction of advection, we anticipate only simple transport of patterns for sufficiently small advection away from any emergent sources or sinks due to the advection.

IV. NUMERICAL SIMULATIONS OF PATTERN FORMATION AND TRANSPORT

Here we numerically simulate Eqs. (1)–(2) using the commercially available finite-element package Comsol. We discretize the sphere of radius R using 19 488 triangular mesh elements. Throughout we take initial data to be equal to the spatially uniform steady state value with a small random perturbation (normally distributed for each element with mean 0 and standard deviation 10^{-3}). We perform convergence checks in space to ensure the accuracy of our simulations by considering simulations with 2800, 6540, 12 556, and 19 488 triangular elements, and noting Cauchy convergence between these discretizations. Similarly, we restricted the maximal time step from $\Delta t_{\max} = 10^{-1}$ to $\Delta t_{\max} = 10^{-3}$ to check convergence in time, and the results from these checks were quantitatively close to results where Comsol was free to choose the time step. Additionally, we used the Matlab package Chebfun to check our results using a very different numerical approach in the case without advection [50,51]. Using identical initial data, we obtain quantitative matching between these implementations.

We begin by analyzing Schnakenberg [43] kinetics and demonstrate some of the behaviors analyzed above. However, in order to demonstrate that these simulations are indicative of generic reaction-advection-diffusion phenomena, rather than anything specific to Schnakenberg kinetics, we consider Geirer-Meinhardt [44] and FitzHugh-Nagumo [45] kinetics as well. In all plots, we only show the concentration of u, as v will have a qualitatively similar pattern (any inexact phase differences, as reported in Ref. [3], are all quite small for the simulations that we have done here and not visually apparent when u and v are plotted alongside one another).

Throughout we will show simulations, and utilize different viewing angles to elucidate the dynamics of spatiotemporal patterns across the sphere. In particular, for unidirectional advection along the x axis, we will denote Regions I, II, and III as in Fig. 2. These correspond to views centered at the two antipodal points (P_1 and P_2) normal to the advection in I and III, and a view of the side of the sphere in II. For other forms of

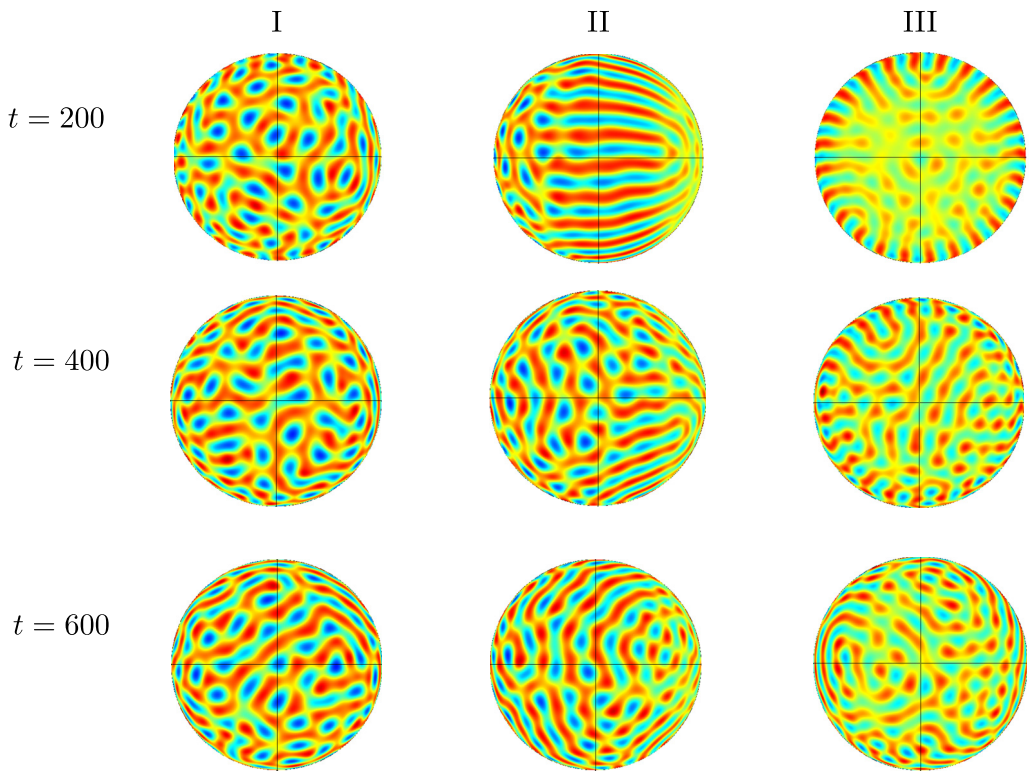

FIG. 3. Formation and transport of labyrinthine patterns in the Schnakenberg model (52) with $R=40$, $a=0.01$, $b=1.2$, $\delta_1=1$, $\delta_2=10$, and $A_x = 0.1$ for $\mathbf{A} = \mathbf{B} = A_x[-\sin(\theta)\sin(\phi), \cos(\theta)\cos(\phi)]$. The three columns are different views of source-side sink, and each row corresponds to $t = 200,400,600$.

the advection vector without such a preferred direction, we will use a common viewing viewing angle centered at the point $\theta = \pi/4$, $\phi = \pi/4$ where both the pole at $\theta = 0$ and the equatorial line at $\theta = \pi/2$ are visible.

A. Schnakenberg reaction kinetics

Schnakenberg reaction kinetics were originally investigated to give a very simple reaction scheme that allowed for limit cycle behavior, by containing a steady state which is an unstable focus [43]. It has been used as a simpler model than the Brusselator in terms of the chemistry being modeled and the analytical tractability of the kinetics. Spot patterns [46,52] and Turing-Hopf bifurcations [47] have been investigated using these kinetics. The range of stationary patterns permissible throughout parameter space is quite large, although in two-dimensional domains, these tend to range from spots to labyrinthine patterns [53]. Due to the underlying oscillatory nature of the kinetics, spiral patterns and pulsing solutions also exist.

The reaction-advection-diffusion system with Schnakenberg reaction kinetics is given by

$$\begin{aligned}\frac{\partial u}{\partial t} &= \frac{\delta_1}{R^2}\triangle u - \frac{1}{R}\nabla\cdot[\mathbf{A}(\mathbf{x})u] + a - u + u^2 v,\\ \frac{\partial v}{\partial t} &= \frac{\delta_1}{R^2}\triangle v - \frac{1}{R}\nabla\cdot[\mathbf{B}(\mathbf{x})u] + b - u^2 v,\end{aligned} \tag{52}$$

where we vary $\mathbf{A}$ and $\mathbf{B}$ as well as the other parameters. We first take $\mathbf{A} = \mathbf{B} = A_x[-\sin(\theta)\sin(\phi), \cos(\theta)\cos(\phi)]$ for a constant A_x which represents the flow induced by an advection in the x direction of an embedding of the sphere into $\mathbb{R}^3$ of magnitude A_x. This can correspond to rheotaxis or convective transport of chemicals (or cells) confined to the surface of a sphere immersed in a fluid, or to a constant magnetic field in the case of magnetotaxis or similar physical scenarios.

In Figs. 2–3 we plot the activator concentration u for this system. This shows transient pattern formation with moderate advection in a parameter regime which admits stable labyrinthine patterns in the advection-free case. The advection affects the transient patterning process by forcing ridges to form in the direction of the advection, before eventually curving and patterning as the nonlinearity takes effect, leading to more familiar labyrinthine patterns in Figs. 2–3. The long-time behavior, shown for a smaller domain with different kinetic parameters in Fig. 4, shows that the labyrinthine pattern originates at one side of the sphere, is transported across it and dissipates at the antipodal point. These points lie at the intersection of the x axis with the sphere. We note that in Figs. 2–4 for both sets of parameters, the local behavior at the "source" (left column) and "sink" (right column) of the sphere is different; the wavelength of pattern appears to be larger near the source, while the sink region appears to destroy patterns by absorbing them into one another around this antipodal point.

In Fig. 5 we show the same long-time behavior, but in a parameter regime where, in the absence of the advection, spot solutions are the typical behavior. As before, the long-time behavior shows the creation and destruction of spot patterns via splitting and coalescence at antipodal points, comparable to some of the transient dynamics discussed in Ref. [19]. Over the circumference of the sphere, the spot patterns appear to be

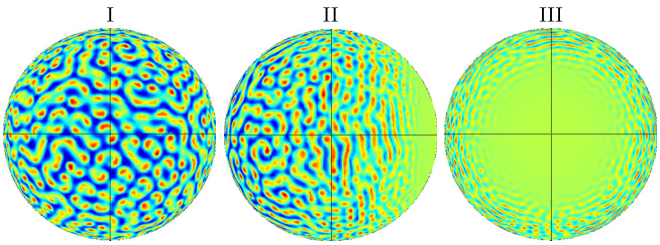

FIG. 4. Long-time ($t = 1000$) dynamics of labyrinthine patterns in the Schnakenberg model (52) with $R = 100$, $a = 0.1$, $b = 0.9$, $\delta_1 = 1$, $\delta_2 = 10$, and $A_x = 4$ for $\mathbf{A} = \mathbf{B} = A_x[-\sin(\theta)\sin(\phi), \cos(\theta)\cos(\phi)]$. The three columns are different views of source-side sink.

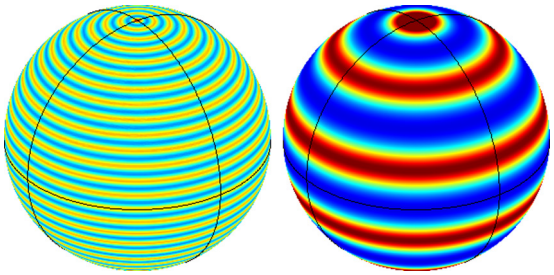

FIG. 6. Final patterns in the Schnakenberg model (52) with $a = 0.1, b = 0.9, \delta_1 = 1$, and $A_\phi = 1$ for $\mathbf{A} = \mathbf{B} = (0, A_\phi)$. On the left we take $\delta_2 = 10$ $R = 100$, and on the right $\delta_2 = 20$ $R = 20$. The view is such that the point $(\pi/4, \pi/4)$ is at the center of the image.

simply transported along by the advection. Analogous comments as in Figs. 2–3 apply to the behavior near the source and sink regions in Fig. 5; spots are larger when they split from one another, and become smaller as they recede into the sink region.

The second case we consider is constant flow in the azimuthal direction, so that $\mathbf{A} = \mathbf{B} = (0, A_\phi)$. In this case, the advection is spinning both species around the sphere at a constant angular velocity. This corresponds to chemical species trapped within a thin shell of viscous fluid being transported by the fluid, if the shell is spinning around the z axis. In this setting, we observe azimuthal transport of patterns independent of their location on the sphere. We note that this case also provides an example of a constant divergence-free advection, as discussed in Sec. II.

In Fig. 6 we give two examples of banded patterns that are oriented along the direction of the advection. These correspond

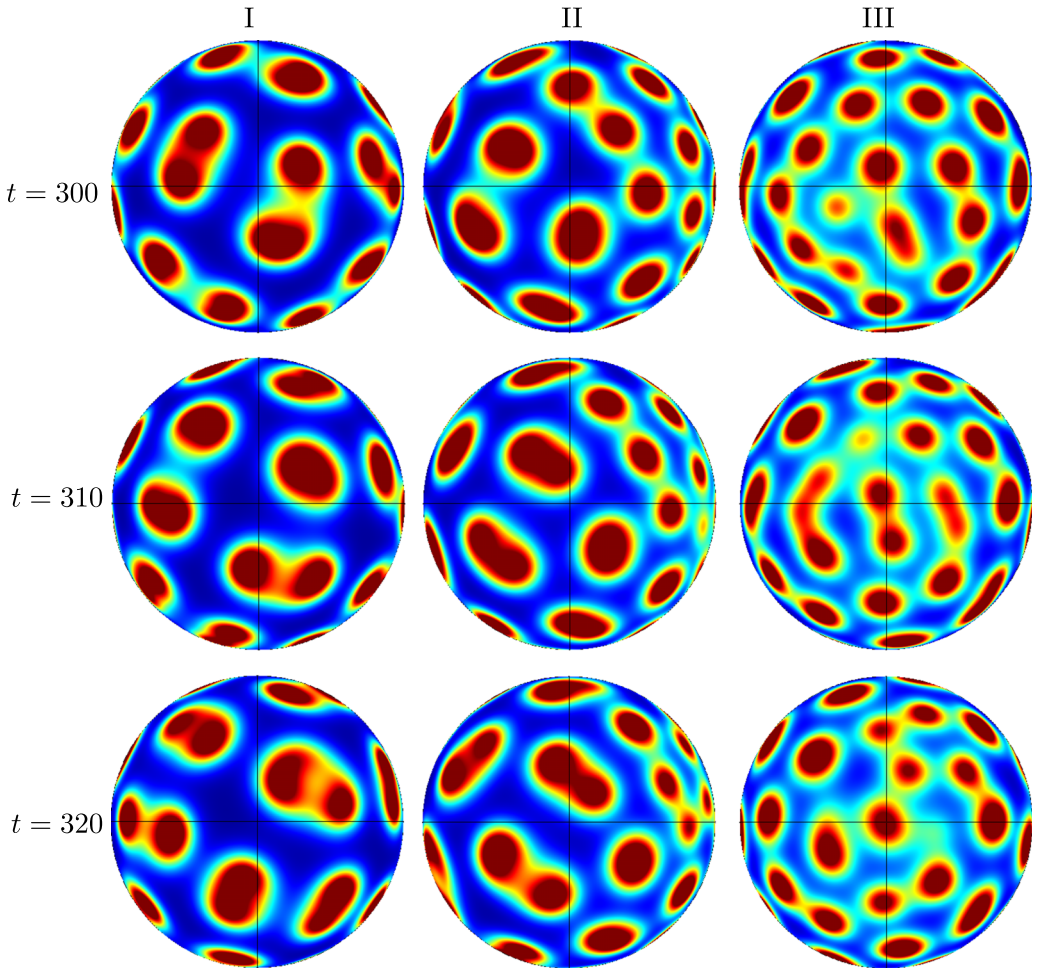

FIG. 5. Long-time movement of spot patterns in the Schnakenberg model (52) with $R = 20$, $a = 0.1$, $b = 0.9$, $\delta_1 = 1$, $\delta_2 = 20$, and $A_x = 0.5$ for $\mathbf{A} = \mathbf{B} = A_x[-\sin(\theta)\sin(\phi), \cos(\theta)\cos(\phi)]$. The three columns are different views of source-side sink, and each row corresponds to $t = 300, 310, 320$.

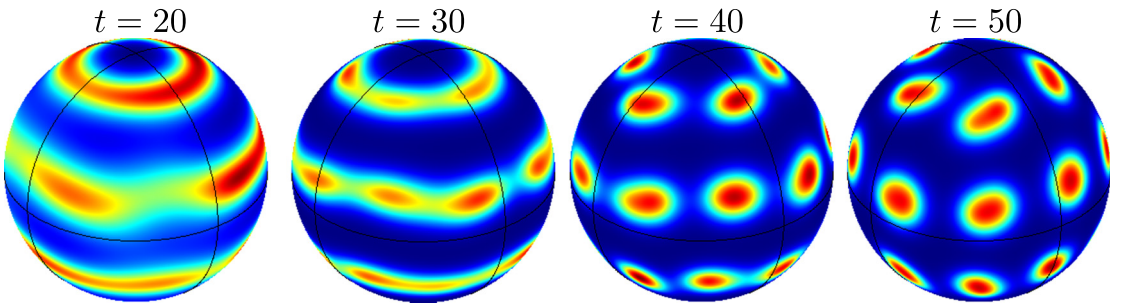

FIG. 7. Transient formation of spot patterns in the Schnakenberg model (52) with $R = 100$, $a = 0.1$, $b = 0.9$, $\delta_1 = 1$, $\delta_2 = 40$, and $A_\phi = 1$ for $\mathbf{A} = \mathbf{B} = (0, A_\phi)$. These are at times $t = 20,30,40,50$. The view is such that the point $(\pi/4,\pi/4)$ is at the center of the image.

to parameters where a planar analog would admit stable spotted patterns and unstable striped patterns. In this case, the advection stabilizes a striped pattern for both parameter sets. Meanwhile, in Fig. 7 we give examples of rotating spot patterns that come from destabilized stripe transients. In particular, we note that the instability from the uniform state resembles the patterns in Fig. 6, but these break up into spot solutions that are transported around the sphere by advection. Small defects and interactions between the spots occur, but the long-time behavior is a simple rotation of a steady state spotted solution.

B. Gierer-Meinhardt reaction kinetics

The Gierer-Meinhardt model was originally proposed as a particular example of Turing's morphogenetic framework [44], based on auto- and cross-catalysis of activator and inhibitor chemicals. This model has been applied to several biological patterning problems, such as the pigmentation and organization of mollusc shells [54]. As in the Schnakenberg system, existence and stability of localized spot patterns has been studied [55], among other solutions.

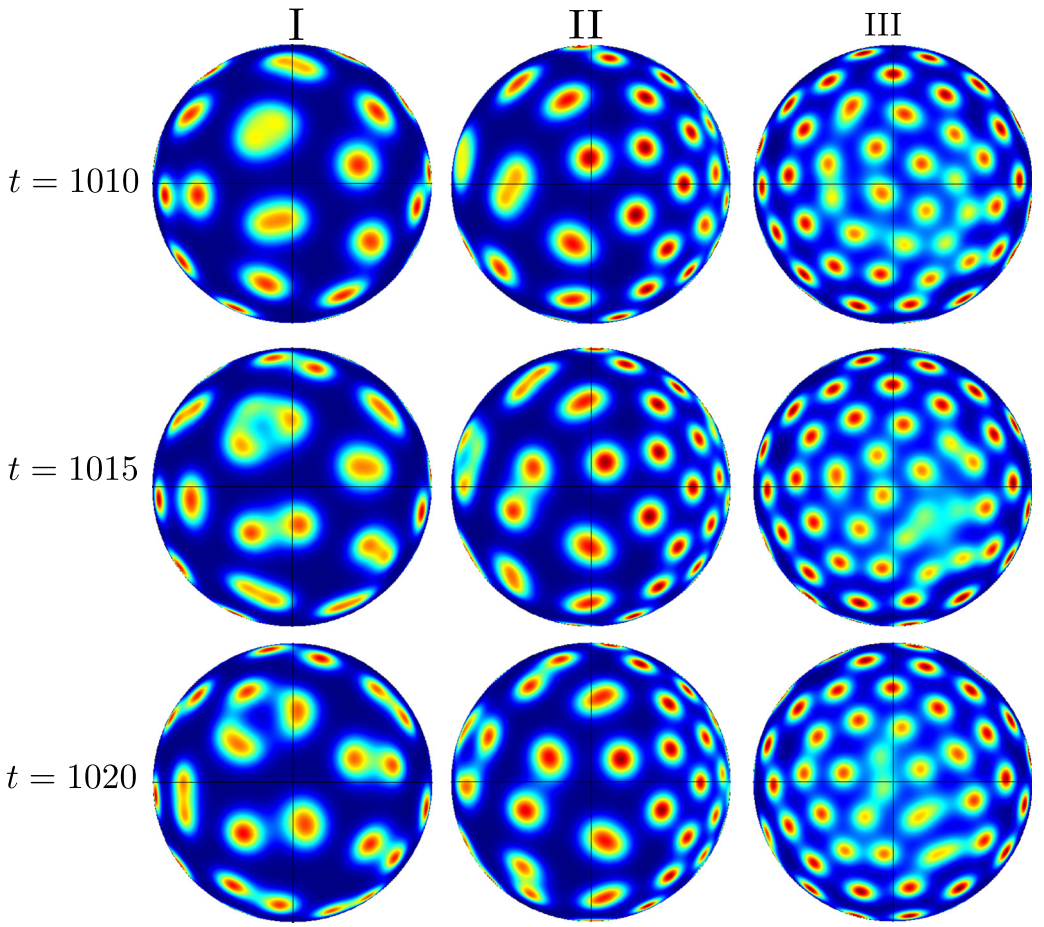

FIG. 8. Long-time movement of spot patterns in the Gierer-Meinhardt model (53) with $R = 20$, $a = 2$, $b = 20$, $\delta_1 = 1$, $\delta_2 = 100$, and $A_x = 0.5$ for $\mathbf{A} = \mathbf{B} = A_x[-\sin(\theta)\sin(\phi), \cos(\theta)\cos(\phi)]$. The three columns are different views of source-side sink, and each row corresponds to $t = 1010,1015,1020$.

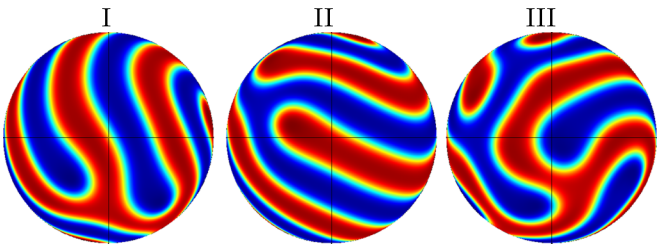

FIG. 9. Steady state patterns in the FitzHugh-Nagumo model (54) with $R = 20, a = 1.2, b = 1.1, \delta_1 = 1, \delta_2 = 20$, and $\mathbf{A} = \mathbf{B} = (0,0)$. The three columns are different views corresponding to $t = 1000$, although in the absence of advection there is no qualitative difference between these regions.

The reaction-advection-diffusion system with Gierer-Meinhardt reaction kinetics is given by

$$\begin{aligned}\frac{\partial u}{\partial t} &= \frac{\delta_1}{R^2}\triangle u - \frac{1}{R}\nabla\cdot[\mathbf{A}(\mathbf{x})u] + \frac{u^2}{v} - au,\\ \frac{\partial v}{\partial t} &= \frac{\delta_1}{R^2}\triangle v - \frac{1}{R}\nabla\cdot[\mathbf{B}(\mathbf{x})u] + u^2 - bv,\end{aligned} \tag{53}$$

with a and b as arbitrary kinetic parameters.

Figure 8 shows a comparable source and sink of spot patterns for the Gierer-Meinhardt system under unidirectional advection comparable to Fig. 5. Localized pulses of activator are generated at one end of the sphere, transported across it, and are destroyed due to an "overcrowding" effect at the other end. It is clearer from this simulation that the sink region is concentrated around a small region around the x axis.

C. FitzHugh-Nagumo reaction kinetics

The FitzHugh-Nagumo kinetics were originally derived to explain the electrical properties of the nerve membrane [45] and can be thought of as a caricature or simplification of the Hodgkin-Huxley model [56]. Since then, it has become a paradigm of excitable media and has been studied from a variety of perspectives. Of particular interest are traveling wave solutions and their physiological implications [2].

The reaction-advection-diffusion system with FitzHugh-Nagumo reaction kinetics is given by

$$\begin{aligned}\frac{\partial u}{\partial t} &= \frac{\delta_1}{R^2}\triangle u - \frac{1}{R}\nabla\cdot[\mathbf{A}(\mathbf{x})u] + u - u^3 - v,\\ \frac{\partial v}{\partial t} &= \frac{\delta_1}{R^2}\triangle v - \frac{1}{R}\nabla\cdot[\mathbf{B}(\mathbf{x})u] + au - bv,\end{aligned} \tag{54}$$

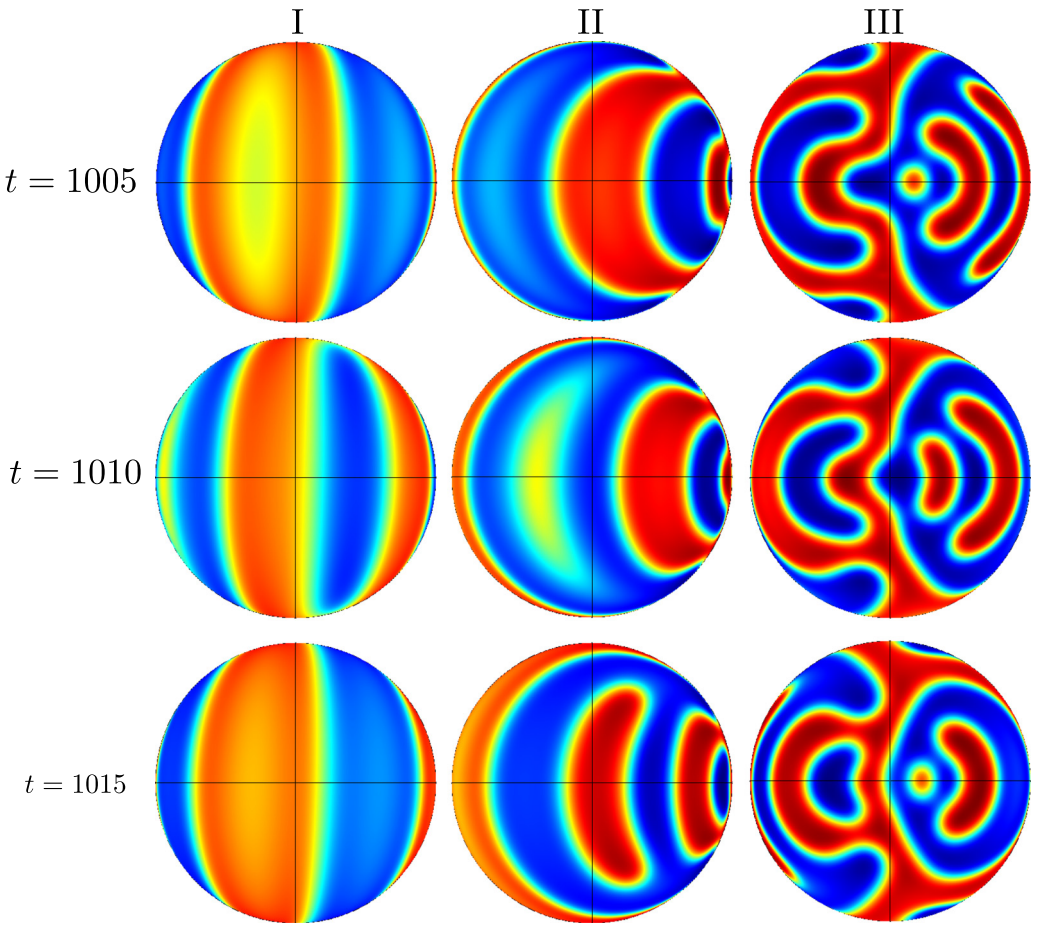

FIG. 10. Long-time movement of wave patterns in the FitzHugh-Nagumo model (54) with $R = 20, a = 1.2, b = 1.1, \delta_1 = 1, \delta_2 = 20$, and $A_x = 1.8$ for $\mathbf{A} = \mathbf{B} = A_x[-\sin(\theta)\sin(\phi), \cos(\theta)\cos(\phi)]$. The three columns are different views of source-side sink, and each row corresponds to $t = 1005, 1010, 1015$.

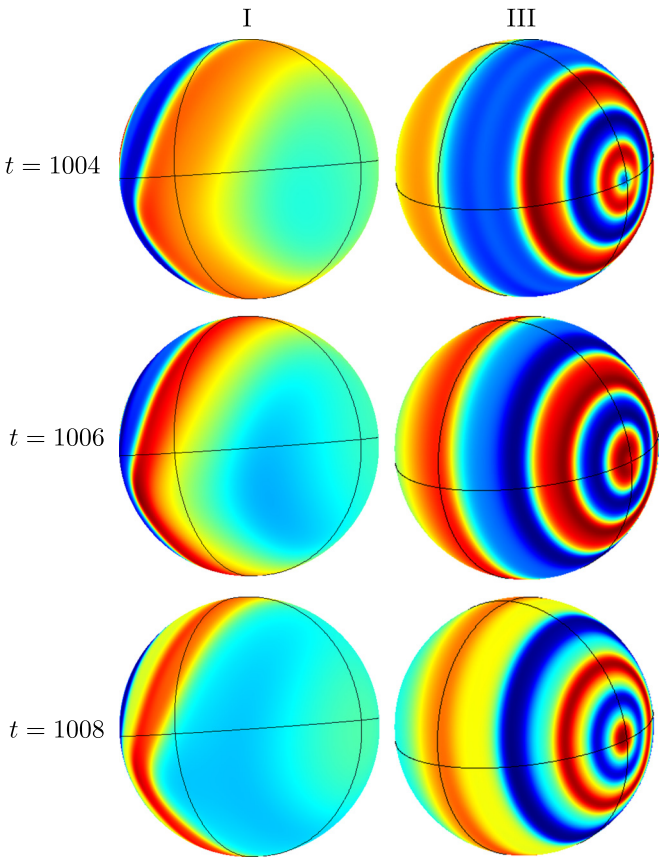

FIG. 11. Long-time movement of wave patterns in the FitzHugh-Nagumo model (54) with $R = 20, a = 1.2, b = 1.1, \delta_1 = 1, \delta_2 = 20$, and $A_x = 1.9$ for $\mathbf{A} = \mathbf{B} = A_x[-\sin(\theta)\sin(\phi), \cos(\theta)\cos(\phi)]$. The two columns are different views with the source on the left and sink on the right, and each row corresponds to $t = 1004, 1006, 1008$. Note that the views have been slanted slightly to observe the formation of the wave at the source, and its disappearance at the sink.

with positive kinetic parameters a and b. To ensure a single uniform steady state, we took $a/b > 1$ in all of our simulations.

Without advection, these patterns settle into a stable labyrinthine state, as shown in Fig. 9. In Fig. 10 we observe traveling bands of of the activator, u, moving across the sphere, with the motion induced by unidirectional advection. In Fig. 11 we give dynamics for slightly larger advection than was considered in Fig. 10, and the dynamics reduce to simple circular waves moving between the source and sink of the pattern. Our results suggest that any value of the advection larger than some critical value will result in dynamics equivalent to this circular wave behavior, implying a bifurcation between qualitatively different traveling wave dynamics on the sphere.

The transient formation of patterns shown in Fig. 10 appears akin to those found in the long-time dynamics of the model with large advection, but quickly breaks up into curved wavefronts resembling traveling labyrinthine structures rather than circular pulses. We also note that the circular waves in Fig. 11 appear to pattern away from the antipodal point to which they are destroyed (where the lines cross on the right side of each diagram). For slightly smaller advection (e.g., Fig. 10) the pattern creation appears to be very local to this singular point where the advection vanishes. As with the previous reaction kinetics, the pattern wavelength and structure are different in the source and sink region.

We ran many other simulations where we varied the presence of advection in each species (e.g., took $\mathbf{B} = \mathbf{0}$ or $\mathbf{A} = \mathbf{0}$), as well as their relative magnitude and sign (e.g., took $\mathbf{B} = c\mathbf{A}$ for some value c). In each case, the qualitative behaviors were similar. An exception to this is the Schnakenberg system, where the advection of the inhibitor v only was typically slower and in the opposite direction of the cases where both advect in the same direction. These results differ from those of differential-flow induced chemical instabilities [12], where differences in the advection between species induced major qualitative changes in the solutions, as these instabilities are different from Turing-type instabilities. In our simulations we were always well within a Turing patterning regime, and so the presence of any advection, differential or equal between species, was not sufficient to change solution behaviors. Near the boundary of the Turing regime we suspect this is no longer true, and different forms of advection could change the dynamics observed, but we leave investigation of this as future work.

D. Translational invariance of localized patterns

We now examine the behavior of steady nonuniform solutions, such as spots, that are seen in nonadvecting reaction-diffusion systems. In a planar reaction-diffusion system, the change of coordinates $\mathbf{x} = \hat{\mathbf{x}} - \mathbf{A}t$ for some constant vector $\mathbf{A}$ transforms nonlinear steady-state solutions in the plane to translating solutions of a reaction-advection-diffusion system. This suggests that translation of patterns is a generic behavior for these kinds of systems, as alluded to in the dynamics of Region II in Sec. III. However, there is no analog of a constant vector field on the sphere.

If we consider purely azimuthal rotation, as in Figs. 7–9, then the advection is of the form $\mathbf{A} = \mathbf{B} = (0, A_\phi)$ for some constant A_ϕ. In this case, we can change variables in Eqs. (1)–(2) via $\hat{\phi} = \phi - \frac{A_\phi}{R\sin(\theta)}t$. In this rotating reference frame, the system is transformed to a standard reaction-diffusion system, and hence, stationary solutions to this system will rotate in the reaction-advection-diffusion system.

Using alternative reference frames and restricting to specific asymptotic regimes, rotation of pulse solutions can be shown explicitly for nonequal advection parameters. Up to restricting advection to lie within various asymptotic regimes, the details in these cases are similar to the planar reaction-diffusion setting (e.g., Refs. [18,55]). However, the stability of such solutions is technically demanding, as demonstrated in Ref. [19], due to the spherical geometry. We do not pursue this here, but suggest it as an area for future application of nonlocal-eigenvalue analysis and other contemporary techniques.

V. DISCUSSION

Motivated by recent mathematical extensions to Turing's original work, we have considered a two-species reaction-advection-diffusion system within the context of a spherical geometry. We have deduced conditions for the instability of a spatially homogeneous solution in a restricted set of parameters, as well as systematically explored several model systems numerically to find interesting behaviors. Some of

these behaviors have planar analogues, but the compact structure of the sphere also appears to give rise to novel behaviors not currently reported in the literature. We find emergent source and sink behavior, rotational translation of spotted and striped patterns, as well as the stabilization and destabilization of various particular nonlinear solutions. Additionally, we suggest a qualitative approach to understanding the source and sink behavior that creates, transports, and destroys patterned regions of the sphere.

We explored many different parameter ranges and functional forms of the advection (including nonlinear advection). Much of the behavior reported in the literature for reaction-advection-diffusion systems on planar domains exhibits analogous behavior in the spherical case. For advection that was either large in magnitude or nonlinear, behaviors varied wildly, but were dependent on the specific nonlinearities and model parameters. We focused on simpler forms of the advection to demonstrate features that we believe are novel and have not been reported in the literature. We leave further investigation of these systems, and in particular a more general and systematic study of nonlinear advection, as future work. The solution behaviors in general will depend heavily on parameters and functional forms for advection and reaction kinetics that depend on a particular physical or biological problem.

One of the most striking features of the reaction-advection-diffusion system on the sphere is the existence of emergent source and sink behaviors due to an interplay between the nonlinear reaction kinetics and the transport due to advection and diffusion. These appear as localized regions where patterns are created, which are then transported across the surface of the sphere to a sink where they are destroyed. We analyzed this behavior in some detail, both because it is indicative of the mathematical difficulties inherent in the problem, and because it is itself an interesting phenomenon. While our analysis does not fully explain the emergent source and sink behaviors we have observed numerically, the local Turing conditions suggest that the regions closest and furthest from a source of advection correspond to fundamentally different spectral problems, which gives some insight into why the patterns in these three regions have qualitatively different properties such as wavelength and amplitude. These results suggest a way of differentiating between local regions on a manifold, where the projection of the system onto local coordinate charts can be used to understand the global dynamical behavior.

Experimentally, reaction-advection-diffusion on compact nonplanar manifolds is likely more realistic as a model for many phenomena, compared to planar reaction-advection-diffusion or to pure reaction-diffusion on a surface. For the model presented in this paper, we have allowed for flows or other physical fields to influence the dynamics constrained to the surface. This allows for a framework capable of modeling a wide range of problems, including geophysical surface flows (as suggested in Ref. [29]), the growth of blastula accounting for local rheology (as originally elucidated by Turing [1]), or surface reactions in many applications (as in Ref. [48] and others, if the bulk reactions are negligible). Additionally, the novel behaviors we have illustrated provide a plethora of mathematical problems to attack, in terms of stability analyses and asymptotic regimes worth considering in further detail than we have done.

[1] A. M. Turing, Philos. Trans. R. Soc. London B **237**, 37 (1952).

[2] J. D. Murray, *Mathematical Biology. II Spatial Models and Biomedical Applications, Interdisciplinary Applied Mathematics* (Springer-Verlag, New York, 2001), Vol. 18.

[3] R. A. Satnoianu and M. Menzinger, Phys. Lett. A **304**, 149 (2002).

[4] P. Andresén, M. Bache, E. Mosekilde, G. Dewel, and P. Borckmanns, Phys. Rev. E **60**, 297 (1999).

[5] G. Bernasconi and J. Boissonade, Phys. Lett. A **232**, 224 (1997).

[6] J. A. Sherratt, Proc. R. Soc. A **467**, 3272 (2011).

[7] L. Kurowski, A. L. Krause, H. Mizuguchi, P. Grindrod, and R. A. Van Gorder, Bull. Math. Biol. **79**, 2302 (2017).

[8] C. R. Nugent, W. M. Quarles, and T. H. Solomon, Phys. Rev. Lett. **93**, 218301 (2004).

[9] D. G. Míguez, R. A. Satnoianu, and A. P. Muñuzuri, Phys. Rev. E **73**, 025201(R) (2006).

[10] E. H. Flach, S. Schnell, and J. Norbury, Phys. Rev. E **76**, 036216 (2007).

[11] T. Nakagaki, H. Yamada, and M. Ito, J. Theor. Biol. **197**, 497 (1999).

[12] A. B. Rovinsky and M. Menzinger, Phys. Rev. Lett. **69**, 1193 (1992).

[13] S. P. Dawson, A. Lawniczak, and R. Kapral, J. Chem. Phys. **100**, 5211 (1994).

[14] M. Núñez-López, G. Chacón-Acosta, and J. Santiago, Braz. J. Phys. **47**, 231 (2017).

[15] C. Varea, J. L. Aragón, and R. A. Barrio, Phys. Rev. E **60**, 4588 (1999).

[16] M. A. J. Chaplain, M. Ganesh, and I. G. Graham, J. Math. Biol. **42**, 387 (2001).

[17] W.-M. Ni and J. Wei, J. Diff. Equ. **221**, 158 (2006).

[18] I. Rozada, S. J. Ruuth, and M. Ward, SIAM J. Appl. Dyn. Syst. **13**, 564 (2014).

[19] P. H. Trinh and M. J. Ward, Nonlinearity **29**, 766 (2016).

[20] H. Levine and W.-J. Rappel, Phys. Rev. E **72**, 061912 (2005).

[21] Y. Schiffmann, Prog. Biophys. Mol. Biol. **95**, 50 (2007).

[22] T. Callahan, Physica D **188**, 65 (2004).

[23] R. G. Plaza, F. Sanchez-Garduno, P. Padilla, R. A. Barrio, and P. K. Maini, J. Dyn. Diff. Equ. **16**, 1093 (2004).

[24] W. H. Tse, J. Wei, and M. Winter, J. Math. Pures Appl. **94**, 366 (2010).

[25] T. Bánsági, V. K. Vanag, and I. R. Epstein, Science **331**, 1309 (2011).

[26] D. L. Williamson and P. J. Rasch, Mon. Weather Rev. **117**, 102 (1989).

[27] P. K. Smolarkiewicz and P. J. Rasch, J. Atmos. Sci. **48**, 793 (1991).

[28] G. Georgiev and G. Iannacchione, Bull. Am. Phys. Soc. **60** (2015).

[29] J. A. Pudykiewicz, J. Comput. Phys. **213**, 358 (2006).

[30] S. M. Burrows, W. Elbert, M. Lawrence, and U. Pöschl, Atmos. Chem. Phys. **9**, 9263 (2009).

[31] S. Burrows, T. Butler, P. Jöckel, H. Tost, A. Kerkweg, U. Pöschl, and M. Lawrence, Atmos. Chem. Phys. **9**, 9281 (2009).
[32] C. A. Kellogg and D. W. Griffin, Trends Ecol. Evol. **21**, 638 (2006).
[33] E. J. Crampin, E. A. Gaffney, and P. K. Maini, Bull. Math. Biol. **61**, 1093 (1999).
[34] R. Barreira, C. M. Elliott, and A. Madzvamuse, J. Math. Biol. **63**, 1095 (2011).
[35] D. Horstmann, J. Nonlinear Sci. **21**, 231 (2011).
[36] T. Hillen and K. J. Painter, J. Math. Biol. **58**, 183 (2009).
[37] H. C. Fu, T. R. Powers, R. Stocker *et al.*, Proc. Natl. Acad. Sci. USA **109**, 4780 (2012).
[38] R. S. Smith, S. Guyomarc'h, T. Mandel, D. Reinhardt, C. Kuhlemeier, and P. Prusinkiewicz, Proc. Natl. Acad. Sci. USA **103**, 1301 (2006).
[39] H. Jönsson, M. G. Heisler, B. E. Shapiro, E. M. Meyerowitz, and E. Mjolsness, Proc. Natl. Acad. Sci. USA **103**, 1633 (2006).
[40] D. Faivre and D. Schuler, Chem. Rev. **108**, 4875 (2008).
[41] M. Marlow, Y. Sasaki, and D. A. Vasquez, J. Chem. Phys. **107**, 5205 (1997).
[42] P. Moon and D. E. Spencer, *Field Theory Handbook: Including Coordinate Systems, Differential Equations and Their Solutions* (Springer, Berlin, 2012).
[43] J. Schnakenberg, J. Theor. Biol. **81**, 389 (1979).
[44] A. Gierer and H. Meinhardt, Kybernetik **12**, 30 (1972).
[45] R. FitzHugh, Bull. Math. Biophys. **17**, 257 (1955).
[46] D. Iron, J. Wei, and M. Winter, J. Math. Biol. **49**, 358 (2004).
[47] P. Liu, J. Shi, Y. Wang, and X. Feng, J. Math. Chem. **51**, 2001 (2013).
[48] A. Madzvamuse, A. H. Chung, and C. Venkataraman, Proc. R. Soc. London A **471**, 20140546 (2015).
[49] M. Abramowitz and I. A. Stegun, *Handbook of Mathematical Functions: With Formulas, Graphs, and Mathematical Tables* (Courier Corporation, New York, 1964), Vol. 55.
[50] A. Townsend and L. N. Trefethen, SIAM J. Sci. Comput. **35**, C495 (2013).
[51] A. Townsend, H. Wilber, and G. B. Wright, SIAM J. Sci. Comput. **38**, C403 (2016).
[52] M. J. Ward and J. Wei, Stud. Appl. Math. **109**, 229 (2002).
[53] W. Sarfaraz and A. Madzvamuse, Chaos, Solitons Fractals **103**, 33 (2017).
[54] H. Meinhardt and M. Klingler, J. Theor. Biol. **126**, 63 (1987).
[55] N. T. Fadai, M. J. Ward, and J. Wei, SIAM J. Appl. Math. **77**, 664 (2017).
[56] A. L. Hodgkin and A. F. Huxley, J. Physiol. **117**, 500 (1952).